NeuroImage 148 (2017) 160–168

Contents lists available at ScienceDirect

NeuroImage

journal homepage: www.elsevier.com/locate/neuroimage

Full Length Articles

Intrinsic signal optical imaging of visual brain activity: Tracking of fast cortical dynamics

Haidong D. Lu[b,c,*], Gang Chen[a,c], Junjie Cai[d], Anna W. Roe[a,c,e]

[a] Interdisciplinary Institute of Neuroscience and Technology, Qiushi Academy for Advanced Studies, Zhejiang University, Hangzhou, China
[b] State Key Laboratory of Cognitive Neuroscience and Learning, Collaborative Innovation Center for Brain Science, Beijing Normal University, Beijing, China
[c] Department of Psychology, Vanderbilt University, Nashville, TN, USA
[d] Institute of Neuroscience, Chinese Academy of Sciences, Shanghai, China
[e] Division of Neuroscience, Oregon National Primate Research Center, Oregon Health & Science University, Beaverton, OR, USA

ARTICLE INFO

Keywords:
Temporal resolution
Intrinsic signal optical imaging
Visual cortex
Monkey
V1

ABSTRACT

Hemodynamic-based brain imaging techniques are typically incapable of monitoring brain activity with both high spatial and high temporal resolutions. In this study, we have used intrinsic signal optical imaging (ISOI), a relatively high spatial resolution imaging technique, to examine the temporal resolution of the hemodynamic signal. We imaged V1 responses in anesthetized monkey to a moving light spot. Movies of cortical responses clearly revealed a focus of hemodynamic response traveling across the cortical surface. Importantly, at different locations along the cortical trajectory, response timecourses maintained a similar tri-phasic shape and shifted sequentially across cortex with a predictable delay. We calculated the time between distinguishable timecourses and found that the temporal resolution of the signal at which two events can be reliably distinguished is about 80 milliseconds. These results suggest that hemodynamic-based imaging is suitable for detecting ongoing cortical events at high spatial resolution and with temporal resolution relevant for behavioral studies.

1. Introduction

Monitoring cortical events with both high spatial and high temporal resolution is crucially important for studying brain function. Most recording and imaging techniques, however, cannot meet both requirements simultaneously. The intrinsic signal optical imaging (ISOI) technique, which measures cortical reflectance change due to hemodynamic response (Grinvald et al. 1986), has high spatial resolution (on the order of 100 μm). Its temporal resolution, however, is believed to be very slow, taking 1–2 s to peak, followed by a long (up to 10 s) return to baseline. Because of this, ISOI is not considered useful for studying fast cortical events.

Our premise in this study is that extended signal timecourses and long delays to peak do not necessarily imply low temporal precision. In fact, we argue that if used properly, significant temporal information can be inferred from the response. Simply put, if two events occur at two different cortical locations with a small onset-time difference, and if the induced response timecourses are similar at the two sites, then the two responses should reach their peak with a similarly small time difference. This would happen regardless of a long delay to peak. Thus the temporal relationship between the two events, even if it is quite small, is faithfully relayed, thereby resulting in a high temporal resolution of event onsets. The limits of detecting such differences can also be determined. Recent fMRI studies have used this rationale to demonstrate that cortical responses can be tracked with high temporal precision using hemodynamic signals. Thus, event-related fMRI has been used not only for brain mapping, but also for tracing the sequence of cortical activation across brain regions during task performance (see review Formisano and Goebel, 2003). However, because the fMRI scanning rate is normally low and the spatial resolution of fMRI signal is on the order of 1 mm, both pose serious limitations on its application for high-spatial, high-temporal resolution brain imaging. In contrast, ISOI has a much higher spatial resolution, with almost unlimited scanning rate, making this approach potentially more suitable for such goals.

Similarly, precise temporal resolution can also be achieved in another hemodynamic-based optical technique, fNIRS (Ferrari and Quaresima, 2012; Scholkmann et al., 2014; Gratton and Fabiani, 2001). fNIRS is a non-invasive optical measurement of brain activity. It uses longer wavelength (650–1000 nm) for better penetration. Due

* Corresponding author at: State Key Laboratory of Cognitive Neuroscience and Learning, Beijing Normal University, Collaborative Innovation Center for Brain Science, Beijing, China.
E-mail address: haidong@bnu.edu.cn (H.D. Lu).

http://dx.doi.org/10.1016/j.neuroimage.2017.01.006
Received 11 August 2016; Accepted 3 January 2017
Available online 04 January 2017

to the influence of skull and scalp, the signal noise ratio and spatial resolution of fNIRS (in the order of 1 cm) is poorer than ISOI. However, the temporal aspects of the origin of these two signals are similar and thus the rational of the precise temporal measurement discussed above still holds. The most important advantage of fNIRS is that it is non-invasive, and thus can be used in human subjects.

Reliability of signal timecourse across different cortical locations is important for this approach. Similar to the signal sources in fMRI and fNIRS, the signal measured in ISOI mainly reflects the overall changes in blood due to neural activation. There are three main sources (blood volume, blood oxygenation, light scattering) that contribute to the overall light reflectance change in ISOI. The amplitude and temporal dynamics of this signal depends on the wavelength of the illumination light and specific stimulus parameters. A large set of studies have shown that, for red light illumination (e.g. 605 nm or 630 nm) the intrinsic signal has a stereotypical response timecourse characterized by an early phase (the initial dip) followed by a large rebound (late positive signal, known as the BOLD in fMRI). Such signals have been observed in both anesthetized (e.g. Frostig et al., 1990; Chen-Bee et al., 2007) and awake preparations (e.g. Vanzetta et al., 2004; Sirotin et al., 2009; Tanigawa et al., 2010).

ISOI signal can also be broken down into global and local response components. The global signal is stimulus-non-specific; the local signal is feature-specific and is confined to functionally specific cortical columns. Many studies have characterized the global signal in response to a point stimulus, including its tri-phasic nature, its point-spread function and the possible underlying hemodynamic components (Chen-Bee et. al., 2007; Sirotin et al., 2009). Temporal features for the local (mapping) signal, however, are less well-understood. In this study we imaged cortical response to moving spot stimuli presented to one eye. We analyzed eye-specific activation (mapping signal) in a 10 s long period after stimulus onset. We found the presence of functionally specific ocular-dominance (OD) signals in all three phases of the hemodynamic responses. This signal appears independent of the global signal, as it does not change its sign with the global signal and lasts longer than the global signal. The timecourses of cortical activation are also similar at different locations. By calculating the timecourse shift along the cortical activation trace, we estimate the temporal resolution limit of ISOI is about 80 ms.

2. Materials and methods

All surgical and experimental procedures conformed to the guidelines of the National Institutes of Health and were approved by the Institutional Animal Care and Use Committees (Institute of Neuroscience, Chinese Academy of Sciences; Vanderbilt University, USA).

2.1. Intrinsic optical imaging

Two Macaque monkeys (*Macaca mulatta*) were used in this study. Monkeys were anesthetized (thiopental sodium, 1–2 mg/kg/hr intravenously [i.v.] and/or isoflurane, 0.2%–1.5%), paralyzed with vecuronium bromide (0.05 mg/kg/hr i.v.), and artificially ventilated. Anesthetic depth was assessed continuously via implanted wire electroencephalographic electrodes, end-tidal CO_2, oximetry, and heart rate, and by regular testing for response to toe pinch while monitoring heart rate changes. A craniotomy and durotomy were performed to expose visual areas V1 and V2 (near the lunate sulcus at an eccentricity of 1–6 degrees from the fovea). Eyes were dilated (atropine sulfate) and fit with contact lenses of appropriate curvature to focus on a computer screen 57 or 76 cm from the eyes. Risley prisms were placed over each eye and eyes were aligned using a rapid retinotopic imaging method (Lu et al., 2009). Alignment was checked before and after each imaging block. The brain was stabilized with agar and images were obtained through a cover glass.

Images of reflectance change (intrinsic hemodynamic signals) corresponding to local cortical activity were acquired with 632 nm illumination (for details, see Roe and Ts'o, 1995; Lu and Roe, 2007). Signal-to-noise ratio was enhanced by trial averaging (usually 20–50 trials per stimulus condition). Frame size was 504×504 pixels and represented 20 mmx20 mm of cortical area. Stimuli were presented in blocks. Each block contained four to nine stimulus conditions presented in a randomly interleaved fashion.

2.2. Visual stimulus

Visual stimuli were created using VSG 2/5 or ViSaGe (Cambridge Research Systems Ltd., Rochester, UK) and presented on a CRT monitor (SONY GDM F500R or CPD-G520). The stimulus screen was gamma corrected. Full screen drifting squarewave gratings were used to obtain basic functional maps including those for ocular dominance, orientation, and color. Spatial and temporal frequencies were optimized for these maps (see Lu and Roe, 2007, 2008).

2.3. Retinotopic grid stimulus

Stationary bar stimuli containing orthogonal squarewave gratings were used for mapping the retinotopy of the imaged V1. Full screen stationary squarewave gratings (SF=1 cycle/deg, duty cycle 0.1) were presented monocularly at two different locations (phase shifted 90 degrees) for 3.5 s each after a 0.5 s delay. Subtraction of these two phase-shifted gratings resulted in a retinotopic map of horizontal or vertical grids (See Fig. 1E & F).

2.4. Moving spot stimulus

A white spot (luminance 60 cd/m^2) was displayed on a black background traveling vertically downward for 4.5 degrees parallel to the vertical meridian. Two traveling speeds (1.5 and 4.5 deg/s) were tested. Spot size was 0.23 degrees and was viewed monocularly. Optical signal was collected for 10 s at 8 Hz, resulting in a total of 80 frames. During the imaging, the first 0.5 s of imaging was collected with no stimulus on the screen for background activity. A spot appeared at time 0.5 second and started to move immediately. The spot disappeared at time 3.5 s (for 1.5 deg/s speed) or 1.5 second (for 4.5 deg/s speed), with a traveling duration of 3 or 1 s, respectively. Each condition was imaged 20 times and results shown are the average of these 20 trials.

2.5. Data analysis

To visualize the cortical response to moving spot, we constructed "single-frame maps". For each frame, the gray value of each pixel was calculated using the following function: $dR/R=(F_x-F_0)/F_0$, in which dR/R represents percent change, F_0 is the average raw reflectance value of the first four frames (taken before stimulus onset and thus representative of the baseline activity), and F_x is the raw reflectance values of the frame under study. Single-frame maps obtained in this way represent the percent intrinsic signal change relative to the initial (pre-stimulus) baseline. Multiple repeated trials were averaged to improve signal-noise ratio.

Cortical functional maps (e.g. Fig. 1D, E, F) were calculated with a standard subtraction method (i.e. difference map, Lu and Roe 2007). Unless otherwise specified, difference maps were clipped at two standard deviations on each side of the median pixel values for display.

The response timecourse is a measurement of how the signal

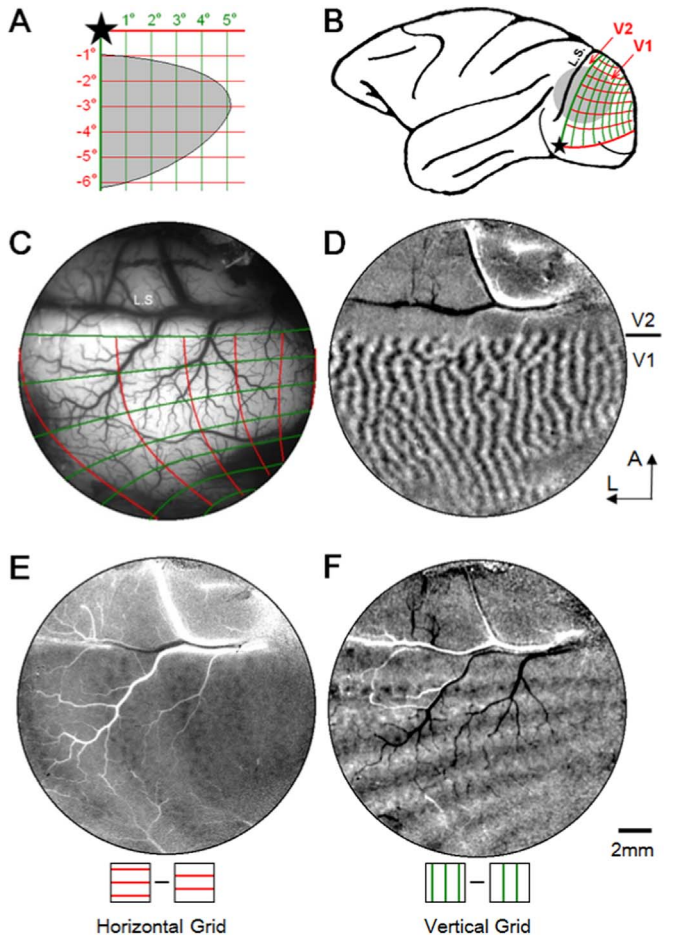

Fig. 1. Determining retinotopic maps in macaque V1. A. Stimulus grid lines presented in lower right visual quadrant for left hemisphere mapping. Star: fovea location. Grid spacing: 1 degree. Line width: 0.1 deg. Gray area: visual field of the imaged field of view in V1 (illustrated in C). B. Location of imaging window (gray disk) on left hemisphere of a macaque brain. Red and green lines correspond to horizontal and vertical grid lines, respectively. L.S.: lunate sulcus. C-F: Cortical images obtained from an imaging window over V1 and V2 (gray disk in B). C. Summary of visual maps imaged in E and F. Surface blood vessel map with imaged retinotopic lines overlaid. Red and green lines correspond to those shown in A. Fovea is out of the window to the left. D. Ocular dominance map (left eye minus right eye subtraction map) illustrating V1/V2 border. A: anterior, L: lateral, applies to C-F. E. A subtraction map of two horizontal grids having 90° phase difference. F. A subtraction map of two vertical grids having 90° phase difference. Scale bar in F: 2 mm applies to C-F. (For interpretation of the references to color in this figure legend, the reader is referred to the web version of this article.)

changes over time. Reflectance change values (dR/R) were first calculated for each pixel and for each frame. Then pixels within a region of interest (e.g. color regions in Fig. 2B) were averaged and plotted against time (e.g. Fig. 2C). No additional filtering was used. To calculate the peak time of each timecourse, a cosine function was fitted to the initial dip and positive rebound and the peak time was calculated from the fitting function.

3. Results

Two macaque monkeys (two hemispheres) were imaged in this study. For each hemisphere, we first obtained basic functional maps of the cortical regions under investigation. These maps include ocular dominance (e.g. Fig. 1D), orientation, color selectivity, motion direction etc. Some functional maps of one case have been previously published (Lu et al. 2010, Fig. 1).

3.1. Mapping retinotopy in V1

Fig. 1 illustrates our mapping procedure. For each imaging field of view (approximate location on brain shown in Fig. 1B, imaged cortical region shown in Fig. 1C), we first demarcate the extent of V1 by identifying the V1/V2 border by ocular dominance mapping (Fig. 1D); this also demarcates the representation of the vertical meridian. Each mapping session began by projecting the optic disk locations onto the stimulus screen to obtain an estimate of the foveal location on the screen (star in Fig. 1A). This foveal estimate then guided the placement of initial spot stimuli used for mapping. We then determined the approximate extent of visual field in the exposed cortical region by using a rapid spot imaging method (Lu et al., 2009). This was determined separately for each eye.

Having more precisely determined the representation within the field of view, we were then able to precisely place grid lines for detailed retinotopic mapping. We imaged cortical response to stationary horizontal and vertical grids through each eye presented in the lower contralateral visual field (Fig. 1A, c.f. Tootell et al. 1988 Figure 7, Blasdel and Campbell 2001, Shmuel et al. 2005): Each line in the grid is 0.1 degree wide and spaced at 1 degree (i.e. 1 cycle/deg gratings). Cortical responses to two phase shifted grid stimuli are subtracted to produce the images shown in Fig. 1E and F. Fig. 1E is a V1 representation of horizontal grids presented to left eye (right eye is covered). For this left hemisphere field of view, foveal representation is toward the left (more lateral). Consistent with this, cortical magnification is larger towards the left than towards the right of the image (larger spacing). Similarly, Fig. 1E, obtained in response to a vertical grid, reveals larger spacing between lines on the left than on the right side of the image. In both Fig. 1E and F, there are approximately 5–6 activation lines in the imaging area, indicating a representation extent of at least 4–5 degrees of visual space. [Note also the patchiness evident within the lines of activation; these are horizontal (1E) and vertical (1 F) orientation domains, also revealed with full field orientation maps.].

A summary map of the overall representation is illustrated in Fig. 1C (red lines: horizontal grid, green lines: vertical grid) overlain on the surface blood vessel map. An extrapolated map on the monkey brain is shown in Fig. 1B, and the extent of the visual field within the chamber is shown in Fig. 1A (gray area, estimated from above analysis). In combination with results from spot imaging (not shown), these retinotopic maps provided accurate visual spatial representation in V1.

3.2. Tri-phasic response to a moving spot

We illustrate an example of the spatiotemporal progression of cortical response to a moving spot (Fig. 2). We imaged cortical responses to a spot moving vertically downward in visual space parallel and close to the vertical meridian. Thus, the activation is expected to move from left to right in the field of view parallel to the V1/V2 border (foveal representation is to left out of field of view). The stimulus was a white spot (0.23 × 0.23 degree square) moving on a black background at a fixed speed of 1.5 degree/s and was viewed monocularly through the left eye. Cortical activation was imaged at 8 Hz frame rate for 10 s. A total of 20 repeats (trials) were averaged. See Movie in supplemental materials (Video S1) as well as on web at ⟨http://www.psy.vanderbilt.edu/faculty/roeaw/spot/ss2_movie-25101.gif⟩. Fig. 2A contains representative frames with time stamps shown at top left corners. Each frame is a dR/R frame representing changes from pre-stimulus baseline (see Method). For the first 5 images (top row), the actual locations of the spot stimulus are estimated (via retinotopic mapping procedure described in Fig. 1) and illustrated on the images as small white circles. The spot appeared at 0.5 s and disappeared at 3.5 second, and thus the white circle is not plotted in the last 5 frames.

Tri-phasic responses are evident in these maps. In the first phase,

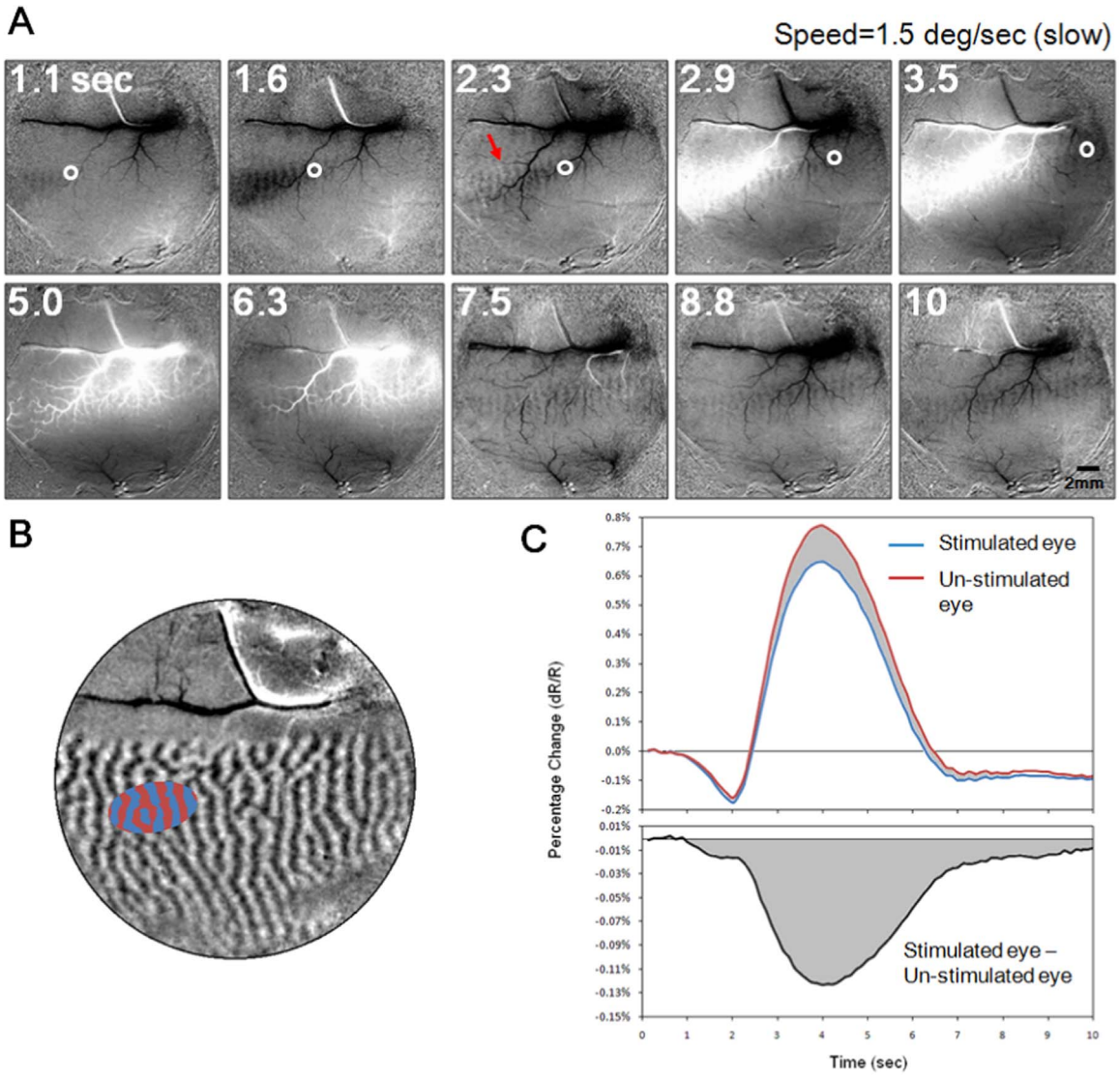

Fig. 2. V1 Response to a moving spot. A. Selected frames from a movie showing optical reflectance change in V1 (and V2) to a spot moving at 1.5 deg/sec. White circles mark the cortical location representing actual location of spot at illustrated time points (indicated at top right corner, in seconds). The moving spot was viewed monocularly, appeared at 0.5 second and disappeared at 3.5 second. Red arrow in 2.3-second frame point to the ocular dominance column corresponding to the stimulated eye (left eye). Images are averaged from 20 trials. Also see Video S1. B. Ocular dominance map (same as shown in Fig. 1F). Blue and red areas are left and right eye domains selected out for detailed timecourse analysis. C. Top: response timecourse of the stimulated eye (blue curve, average of blue pixels in B) and the non-stimulated eye (red curve, average of red pixels in B) in response to the moving spot. Bottom: the difference of the red and blue curves: stimulated (blue) minus un-stimulated (red) eye domains. Cortical response to moving spot shows tri-phasic response. Eye specific information (bottom) persists into period of late negative undershoot. This domain-specific signal is always negative. (For interpretation of the references to color in this figure legend, the reader is referred to the web version of this article.)

during what would correspond to the initial dip period (0–2 s post stimulus onset), a darkening appears. Note the spot first appeared outside the field of view. The spatial distance between this darkening region and the actual stimulus location (white circle) represents the temporal delay between the hemodynamic signal and stimulus onset (about 1–2 s). Importantly, within this darkening region are evident ocular dominance (left eye) columns (e.g. red arrow in the 2.3 s frame).

In the second phase (approx. 3–6 s), we observe a large patch of whitening which extends across a large mediolateral spatial extent. This whitening is the positive rebound of the hemodynamic signal presumably associated with the positive BOLD. Note that this whitening signal is closely associated with the large vasculature. During this phase, ocular dominance columns, although partially obscured by the large positive signal, are still present.

In the third phase (approx. 7–10 s), we observe an undershoot which lingers long after the stimulus disappears. In this stimulus condition, the stimulus disappears at 3.5 s. The last frame in Fig. 2A (time 10 s) which still contains the undershoot is imaged 6.5 s after the stimulus offset. Ocular dominance columns remain evident during this third phase.

By observing the entire 10 s cortical activation sequence, we note that at any given time, different regions along the trace contain different phases of this spatiotemporal activation pattern. Due to temporal smearing, cortical activation is elongated along the spot trajectory. These activation maps reveal important points. First, if one observes the darkening signal, there is clearly ocular dominance structure, indicating the negative signal is spatially specific. However, if one observes the whitening signal, it is, in contrast, highly vascular, with less obvious ocular dominance structure and appears less spatially specific. Thus, the darkening and whitening components of the signal appear to have different spatial specificities. Second, it is evident that the functionally specific signal is long-lasting. Visually, left-eye-specific

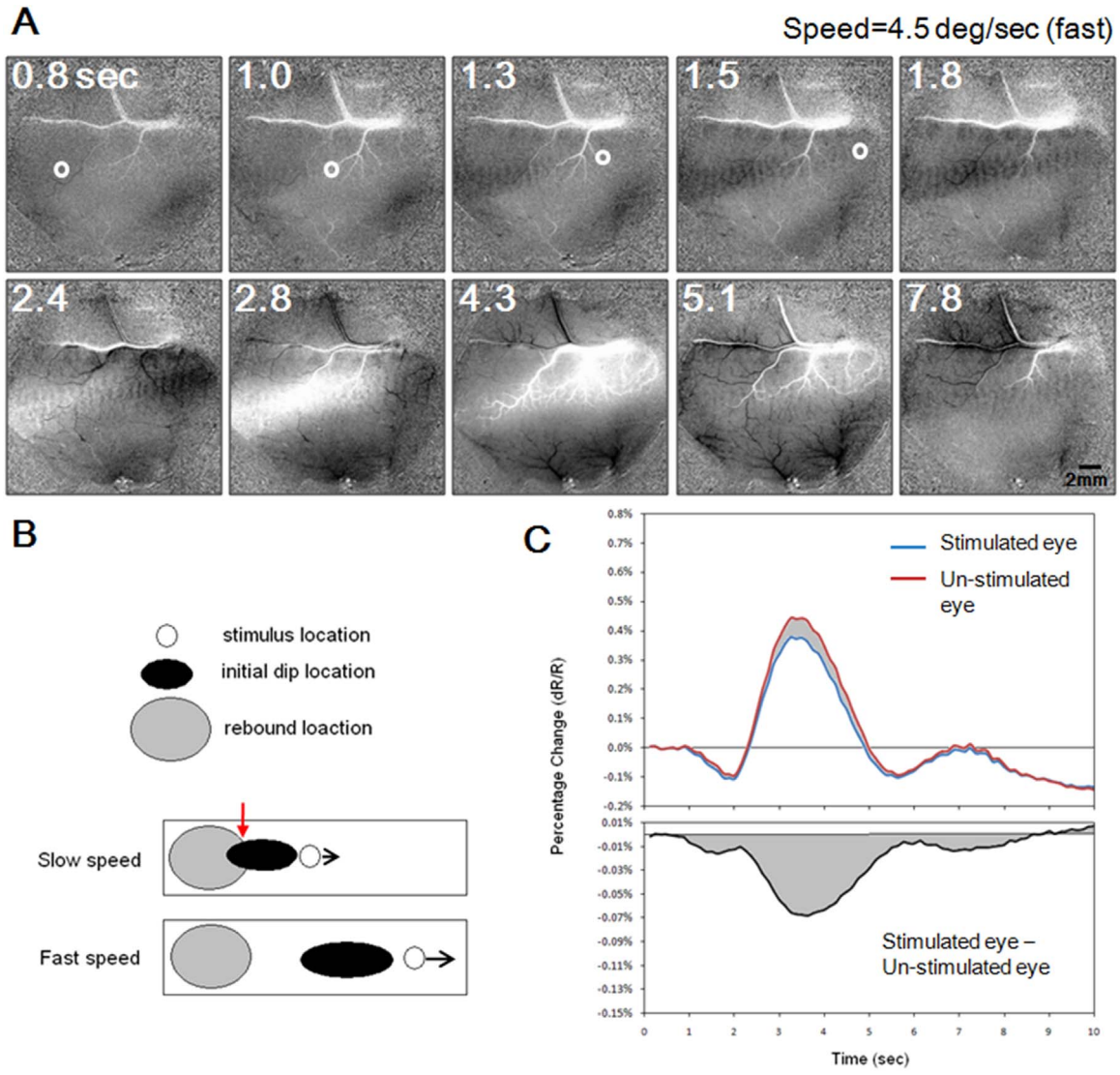

Fig. 3. V1 Response to a fast moving spot. Conventions same as Fig. 2 except dot speed is 4.5 deg/sec. Spot appeared at 0.5 second and disappeared at 1.5 second. A and C are plotted with the same conventions as A and C in Fig. 2. B: Schematic illustrating spatial interactions between initial dip signal (black oval) and late positive rebound signal (gray oval). Stimulus location is represented as a white circle. At slow speed, the initial dip and late positive signal share spatial overlap (red arrow); at faster speed, these two signals are largely segregated which permit better temporal estimation. C: Similar to responses to a slow speed dot (Fig. 2C), the global signal is tri-phasic (top panel) and domain-specific signal is always negative (bottom panel). (For interpretation of the references to color in this figure legend, the reader is referred to the web version of this article.)

domains (black vertical stripes) are most obvious in the initial dip and late undershoot periods (e.g. at 1.6 and 7.5 s) and less clear, but still present, during the period of positive rebound.

To analyze the timecourse of the response in detail, we selected an oval region located on the path of the traveling spot. Fig. 2B shows the ocular dominance map and the oval region selected. The size of this region is close to the size of the V1 response to a stationary spot of 0.25° in size (see Lu et. al., 2009). To improve the signal/noise ratio, pixels belonging to the left eye columns (blue) and the right eye columns (red) are averaged to generate two timecourses. The time-dependent changes of pixel values (dR/R) are plotted in Fig. 2C. The overall response (global signal) from both stimulated eye domains (blue curve) and non-stimulated-eye domains (red curve) shows a clear tri-phasic pattern: a negative initial dip (0.5–2.5 s), a large positive rebound (2.5–6.5 s), and a late negative undershoot (6.5–10 sec).

Although only one eye is stimulated, the differences between these two curves are small, indicating the majority of the signal is stimulus non-specific. This is likely caused both by the fact that the majority of V1 neurons are binocular and by the spatial non-specificity of the underlying hemodynamic signal. Both of these two factors contribute to the common part of the two curves (so called global signal). Interestingly, the blue curve (representing the stimulated eye) is always below the red curve (non-stimulated eye), indicating that the eye-specific signal is always negative. The differential curve in the bottom panel in Fig. 2C also clearly shows that, throughout this 10 s imaging period, the left eye activation is consistently more negative than the right-eye activation, and this relationship remains even after the overall reflectance has returned to the baseline. Thus, importantly, the domain-specific signal is always negative (Fig. 2C bottom, cf. Moon et al., 2007).

3.3. Temporal resolution

To study the temporal resolution of cortical activation, we compared the spatiotemporal profile of spots moving at two different speeds. Fig. 3 illustrates movie frames of a faster moving spot (4.5 deg/s). The 5 frames in the top row in Fig. 3A represent events occurring within the initial 2 s. Cortical response to the spot is strong even

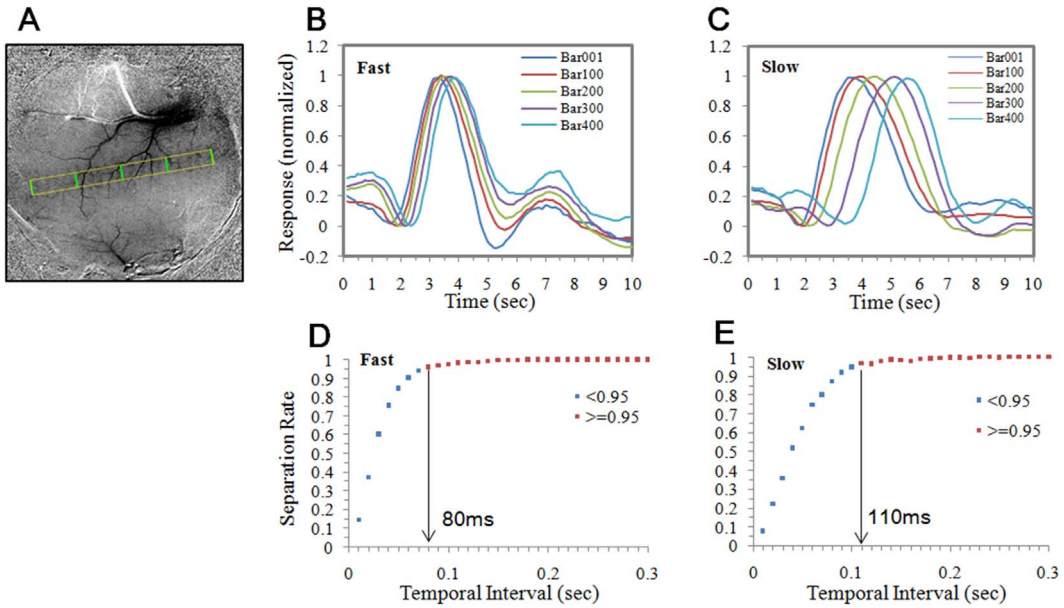

Fig. 4. Estimation of temporal resolution limit. The data set is from the same case as shown in Figs. 2 and 3. A. A negative undershoot frame (the 10-second frame in Fig. 2A) was used to illustrate the trajectory of the moving dot (yellow rectangle). Five equally-spaced lines (green lines) were selected in V1. The response timecourses of the pixels underlying these lines were calculated from fast and slow spot conditions and shown in B and C, respectively. Traces were normalized to amplitude of rebound peak minus initial dip peak. The timecourses at different points along the trajectory show similar temporal shapes and systematic shifts in the time axis. Multiple pairs having the same temporal separation can be selected from the trajectory and used for calculating the probability of successful separation. D & E: The percentage of the pairs having the same temporal separation (X axis) that their timecourses are statistically separable. For fast moving dots, over 95% of pairs separated by 80 ms can be separated. For slow moving dots, this value is larger (110 ms). See text for details. (For interpretation of the references to color in this figure legend, the reader is referred to the web version of this article.)

though the exposure of each cortical location to the stimulus is quite brief (~0.2 s). Compared with the spot traveling at lower speed (Fig. 2), both the initial dip (e.g. at 1.8 s) and the positive rebound (e.g. at 2.8 s) show a more elongated response pattern along the path. This greater elongation is due to the fact that the spot traveled a longer distance in each frame (about 0.56 degrees each frame for the speed of 4.5 degree/s, compared with 0.19 degrees each frame for 1.5 degree/s). Although different in speeds, the temporal delay between initial dip and positive rebound is similar for the fast and slow moving spots (~2 s). In the fast moving spot condition, this temporal separation should result in less interference (spatial overlap) between the initial dip signal and the positive rebound (schematically illustrated as black and gray, respectively, in Fig. 3B). Such interference between initial dip and rebound will shift the peak locations both spatially and temporally and lead to inaccuracy of spatial and temporal judgments. The average timecourses of the fast moving spot are shown in Fig. 3C (averaged from 20 trials) using the same plotting convention as in Fig. 2C. Due to shorter activation time, cortical responses to the faster moving stimulus are smaller in amplitude and last for a briefer period of time. However, the same tri-phasic response timecourses are still evident. Since images obtained from faster spot contain less spatial interference between different temporal components, response from the faster spot may provide more accurate temporal resolution estimates.

To assess temporal resolution, we selected a 30×400 pixel rectangular region over the trajectory of the moving dot (yellow outline in Fig. 4A). Two sets of representative timecourses, averaged from the pixels under the green lines in Fig. 4A, are shown for both fast (Fig. 4B) and slow (Fig. 4C) dot conditions. (Note that, unlike Figs. 2C and 3C, pixels from both eye domains were averaged.) It is clear that normalized timecourses from different cortical regions show similar tri-phasic pattern, and are shifted along the time axis. The temporal activation profile at each location is constant across cortex and serves as a fundamental template for hemodynamic cortical response.

For a pair of lines that are a large distance apart (e.g. any pair of lines in Fig. 4A), it is clear that their temporal timecourses are separable (Fig. 4C). We then calculated how close two timecourses need to be to make them statistically inseparable. This minimum detectable shift then reflects the temporal resolution for sequential events occurring across cortex surface. By selecting any two lines within the trajectory rectangle, we obtained two sets of pixels, each has a trial-averaged timecourses. We then calculated the rebound peak locations for each of these timecourses. The separability of these two groups of peak times was evaluated with a t-test ($p < 0.05$, one-tailed). For each temporal separation, we evaluated many (~200) such pairs along the trajectory. The probability of separating two pairs is increased when two locations are further apart. Fig. 4D and E shows the percentage (Y axis) of the pairs having the same distance (X axis) that are statistically separable. For fast moving dots (Fig. 4D), over 95% of pairs are separable at 80 ms time difference. For slow moving dots (Fig. 4E), this value is larger (110 ms), probably due to interference between different phases of the initial dip and rebound signals.

4. Discussion

In this study we demonstrate that the temporal structure of intrinsic optical responses to a moving spot is very similar at different time points (and cortical locations) in V1. This permits the extraction of stimulus timing information by comparing temporal delays. The hemodynamic-based imaging technique, therefore, can be used in certain studies where high (~100 ms) temporal resolution is needed. We also demonstrate that domain-specific signals in intrinsic optical responses are persistently negative (Figs. 2C and 3C).

4.1. Temporal precision of the intrinsic signal

Imaging cortical response to a moving object has been successfully achieved with voltage sensitive dye methods (Jancke et al., 2004). In their study, cortical waves induced by a moving spot were observed in cat visual cortex. Imaging cortical waves based on intrinsic signals, however, has not yet been demonstrated. Although the intrinsic optical

signal has a long delay and takes a long time to return to baseline, its temporal structure is rather fixed for similar stimuli at different locations. This phenomenon has been shown in previous studies using stationary stimuli (Frostig et al., 1990; Chen-Bee et al., 2007). It means that useful timing information can be extracted from the onset latencies and peak latencies. In this study, we showed that movies of cortical response faithfully represent a fast moving object in the visual space. Furthermore, the traveling speed of cortical response can be calculated with high precision. For spots moving at relatively low speeds (1.5 deg/s), it is very likely that the first two phases of response (which are opposite in sign) mix to a certain degree (see Fig. 2A at 2.3 s). Our interpretation is that the late coming positive rebound drives the overall signal to more positive values, making the apparent peak time of the initial dip peak earlier than it otherwise would be. It has been shown that when use shorter wavelength (e.g. 530 nm) as illumination light in ISOI imaging, the responses are always negative (Sirotin et al., 2009), and interactions between the first and second phases of response can be avoided. We predict that a better temporal precision can be achieved when a shorter wavelength is used.

The temporal precision measured in the present study is from an anesthetized preparation. In awake conditions, the signal strength will increase while noise also increases (Roe, 2007), how they affect the temporal precision measurement is not clear. However, under anesthetized condition, visual cortex is mainly driven by bottom-up (stimulus-driven) activity. In awake conditions, there might be contamination from top-down signals (e.g. anticipation, see Sirotin and Das, 2009.) which add additional variables to the signals and the temporal measurement maybe less accurate. The temporal dynamics of these top-down related variables are themselves interesting topics and can be studied with ISOI (see discussion below).

4.2. Potential applications and significance

The advantage of the intrinsic signal over voltage sensitive dye signal is that it involves no staining with dyes. Given its potential for tracking fast changing events, ISOI can be used not only to image response to a moving object, but also for other types of cortical dynamics. The temporal resolution achieved in this study (80 ms) can be further improved by including more pixels into comparison samples (the green lines in Fig. 4A). Furthermore, all hemodynamic signal based imaging, including fMRI and fNIRS, can use the same methodology to achieve high temporal resolution. With enough repeats and pixels (or voxels), we predict that even higher resolution should be achievable, or less repeats are required. For example, by averaging many eye-specific pixels in V1, a recent study in anesthetized monkey V1 has demonstrated that on-going dynamics of eye-specific signals can be measured in single-trial ISOI imaging (Xu et al., 2016).

However, some precautions must be taken when applying this method. Importantly, to reliably calculate temporal offsets between two cortical locations, the shapes of their signal timecourses must be the same. That is, the assumption that the same hemodynamic response is obtained at different cortical locations must hold. In the present study, we used the same stimuli (moving dot) in a relatively homogenous cortical area (V1), thus stereotypical response timecourses were obtained for the delay calculation. When different types of stimuli are used, or the spatial separation is large (or between two different areas), the differences between their timecourse shapes must be considered. Alternatively, one can study the factors that modulates the temporal shape of the timecourse, for example, by measuring the activity in the same cortical regions during different behavioral tasks.

After these limitations are considered, ISOI/fMRI/fNIRS can be appropriate for studying perceptual events such as filling-in, tracking patterns of cortical motor response, and behavioral and cognitive studies such as attentional modulation (e.g. attend vs. ignore). Potential for use in studying functional connections based on the difference in feed forward and feedback timing is also on the horizon (Ahmed et al., 2008).

4.3. Tri-phasic response

Previous studies have shown multiple phases in intrinsic optical imaging. Chen-Bee et al. (2007) studied rat barrel cortex activation in response to a one-second whisker stimulation with 635 nm illumination. They found three phases in the signals: an initial dip, then a positive overshoot, followed by a negative undershoot. In awake fixating monkeys, Sirotin et al. (2009) demonstrate tri-phasic response in V1 under 605 and 630 nm illumination, but not for 530 nm. Here we also found three such phases in the moving spot activation. The similarity between these two studies indicates the common cortical hemodynamic activity in response to sensory stimulation. Consistent with previous findings (e.g. Fig. 1D in Vanzetta et al., 2004), we show that domain-specific signal (the ocular dominance signal) is constantly negative and lasts through the three phases (initial dip – rebound – undershoot) of the global signal. This also means that the subtraction map does not change its sign even though the sign of the original signal (dR/R) reversed twice during the tri-phasic period. Furthermore, the lingering domain-specific signal in the late undershoot is interesting, as it remains long after the stimulus has disappeared. Although it is possible that this late response is due to an associated “afterimage” (due to the high contrast and small size of the stimulus), studies of rat barrel cortex suggest that such long lasting signal may not be related to neuronal activity (Chen-Bee et al., 2007). By decomposing the underlying hemodynamic components of the intrinsic signal using different wavelengths of illumination, Sirotin et al. (2009) suggests that this late darkening is dominated by slowly decaying of blood volume (i.e. total hemoglobin), rather than a late increase in deoxyhemoglobin. However, how such a signal remains so local (domain-specific) for so long is still not clear.

Acknowledgements

We thank Lisa Chu for surgical assistance and Jie Lu for imaging processing assistance. This work was supported by National Natural Science Foundation of China (31371111, 31530029, 31625012) to HDL; National Natural Science Foundation of China (31471052), Fundamental Research Funds for the Central Universities (2015QN81007), Zhejiang Provincial Natural Science Foundation of China (LR15C090001) to GC; NIH grant EY11744, National Natural Science Foundation of China (key project No. 81430010), National Hi-Tech Research and Development Program of China (No. 2015AA020515) to AWR; Vanderbilt Vision Research Center, and Vanderbilt University Center for Integrative & Cognitive Neuroscience.

Appendix A. Supplementary material

The following are the supplementary data to this article: Video S1 Video S2.

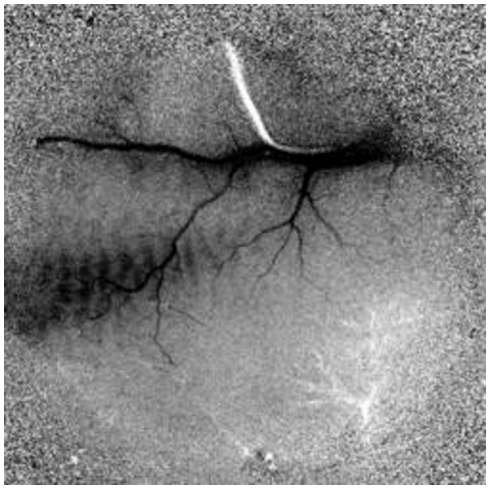

Video S1. Cortical hymodynamic responses to a moving spot. This ten-second movie shows V1 responses to a 0.23 degree light spot traveling (speed 1.5 deg/sec) across the visual field of one eye. Imaging frame rate was 8 Hz. Each frame is a dR/R frame averaged over 20 trials. A video clip is available online.Supplementary material related to this article can be found online at http://dx.doi.org/10.1016/j.neuroimage.2017.01.006.

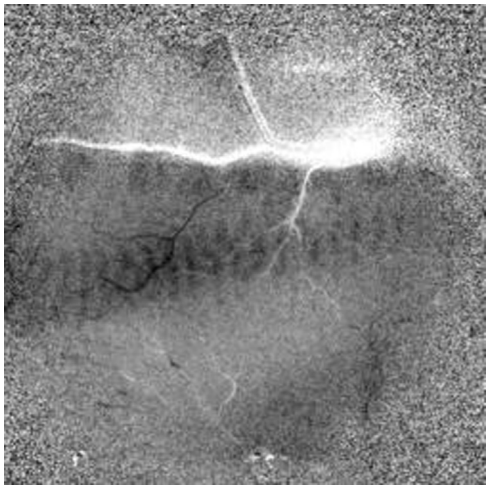

Video S2. The same experimental settings as in Movie 1, except that the dot speed is 4.5 deg/sec in this imaging. A video clip is available online.Supplementary material related to this article can be found online at http://dx.doi.org/10.1016/j.neuroimage.2017.01.006.

References

Ahmed, B., Hanazawa, A., Undeman, C., Eriksson, D., Valentiniene, S., Roland, P.E., 2008. Cortical dynamics subserving visual apparent motion. Cereb. Cortex 18, 2796–2810.

Blasdel, G., Campbell, D., 2001. Funcrtional retinotopy of monkey visual cortex. J. Neurosci. 21, 8286–8301.

Chen-Bee, C.H., Agoncillo, T., Xiong, Y., Frostig, R.D., 2007. The triphasic intrinsic signal: implications for functional imaging. J. Neurosci. 27, 4572–4586.

Ferrari, M., Quaresima, V., 2012. A brief review on the history of human functional near-infrared spectroscopy (fNIRS) development and fields of application. Neuroimage 63 (2), 921–935.

Formisano, E., Goebel, R., 2003. Tracking cognitive processes with functional MRI mental chronometry. Curr. Opin. Neurobiol. 13, 174–181.

Gratton, G., Fabiani, M., 2001. Shedding light on brain function: the event-related optical signal. Trends Cogn. Sci. 5 (8), 357–363.

Grinvald, A., Lieke, E., Frostig, R.D., Gilbert, C.D., Wiesel, T.N., 1986. Functional architecture of cortex revealed by optical imaging of intrinsic signals. Nature 324, 361–364.

Frostig, R.D., Lieke, E.E., Ts'o, D.Y., Grinvald, A., 1990. Cortical functional architecture and local coupling between neuronal activity and the microcirculation revealed by in vivo high-resolution optical imaging of intrinsic signals. Proc. Natl. Acad. Sci. U. S. A. 87, 6082–6086.

Jancke, D., Chavane, F., Naaman, S., Grinvald, A., 2004. Imaging cortical correlates of illusion in early visual cortex. Nature 428, 423–426.

Lu, H.D., Roe, A.W., 2007. Optical imaging of contrast response in Macaque monkey V1 & V2. Cereb. Cortex 17, 2675–2695.

Lu, H.D., Chen, G., Ts'o, D.Y., Roe, A.W., 2009. A rapid topographic mapping and eye alignment method using optical imaging in Macaque visual cortex. Neuroimage 44, 636–646.

Lu, H.D., Roe, A.W., 2008. Functional organization of color domains in V1 and V2 of Macaque monkey revealed by optical imaging. Cereb. Cortex 18, 516–533.

Lu, H.D., Chen, G., Tanigawa, H., Roe, A.W., 2010. A motion direction map in Macaque V2. Neuron 68, 1002–1013.

Moon, C.-H., Fukuda, M., Park, S.-H., Kim, S.-G., 2007. Neural interpretation of blood oxygenation level-dependent fMRI maps at submillimeter columnar resolution. J. Neurosci. 27, 6892–6902.

Tootell, R.B., Switkes, E., Silverman, M.S., Hamilton, S.L., 1988. Functional anatomy of macaque striate cortex. II. Retinotopic organization. J. Neurosci. 8, 1531–1568.

Roe, A.W., 2007. Long-term optical imaging of intrinsic signals in anesthetized and awake monkeys. Appl. Opt. 46 (10), 1872–1880.

Roe, A.W., Ts'o, D.Y., 1995. Visual topography in primate V2: multiple representation across functional stripes. J. Neurosci. 15, 3689–3715.

Scholkmann, F., Kleiser, S., Metz, A.J., Zimmermann, R., Mata Pavia, J., Wolf, U., Wolf, M., 2014. A review on continuous wave functional near-infrared spectroscopy and imaging instrumentation and methodology. Neuroimage 85 (1), 6–27.

Shmuel, A., Korman, M., Sterkin, A., Harel, M., Ullman, S., Malach, R., Grinvald, A., 2005. Retinotopic axis specificity and selective clustering of feedback projections from V2 to V1 in the owl monkey. J. Neurosci. 25, 2117–2131.

Sirotin, Y.B., Das, A., 2009. Anticipatory haemodynamic signals in sensory cortex not predicted by local neuronal activity. Nature 457 (7228), 475–479.

Sirotin, Y.B., Hillman, E.M., Bordier, C., Das, A., 2009. Spatiotemporal precision and hemodynamic mechanism of optical point spreads in alert primates. Proc. Natl.

Acad. Sci. U. S. A. 106, 18390–18395.
Tanigawa, H., Lu, H.D., Roe, A.W., 2010. Functional organization for color and orientation in macaque V4. Nat. Neurosci. 13, 1542–1548.
Vanzetta, I., Slovin, H., Omer, D.B., Grinvald, A., 2004. Columnar resolution of blood volume and oximetry functional maps in the behaving monkey; implications for FMRI. Neuron 42, 843–854.
Xu, H., Han, C., Chen, M., Li, P., Zhu, S., Fang, Y., Hu, J., Ma, H., Lu, H.D., 2016. Rivalry-like neural activity in primary visual cortex in anesthetized monkeys. J. Neurosci. 36, 3231–3242.